SMC-TR-94-15

AEROSPACE REPORT NO.
TR-0091(6940-05)-11

Electron and Proton Wide-Angle Spectrometer (EPAS) on the CRRES Spacecraft

15 March 1994

Prepared by

A. KORTH, G. KREMSER, B. WILKEN, and W. GÜTTLER
Max-Planck-Institute für Aeronomie

S. L. ULLALAND
University of Bergen

and

R. KOGA
Space and Environment Technology Center
Technology Operations
The Aerospace Corporation

Prepared for

SPACE AND MISSILE SYSTEMS CENTER
AIR FORCE MATERIEL COMMAND
2430 E. El Segundo Boulevard
Los Angeles Air Force Base, CA 90245

Engineering and Technology Group

This report was submitted by The Aerospace Corporation, El Segundo, CA 90245-4691, under Contract No. F04701-88-C-0089 with the Space and Missile Systems Center, 2430 E. El Segundo Blvd., Suite 6037, Los Angeles AFB, CA 90245-4687. It was reviewed and approved for The Aerospace Corporation by A. B. Christensen, Principal Director, Space and Environment Technology Center. Maj. Leslie O. Belsma was the project officer for the Mission-Oriented Investigation and Experimentation (MOIE) program.

This report has been reviewed by the Public Affairs Office (PAS) and is releasable to the National Technical Information Service (NTIS). At NTIS, it will be available to the general public, including foreign nationals.

This technical report has been reviewed and is approved for publication. Publication of this report does not constitute Air Force approval of the report's findings or conclusions. It is published only for the exchange and stimulation of ideas.

LESLIE O. BELSMA, MAJ, USAF
MOIE Project Officer

WILLIAM KYLE SNEDDON, CAPT, USAF
Deputy Chief
Industrial and International Division

REPORT DOCUMENTATION PAGE

Form Approved
OMB No. 0704-0188

1. AGENCY USE ONLY (*Leave blank*)	2. REPORT DATE	3. REPORT TYPE AND DATES COVERED
	15 March 1994	

4. TITLE AND SUBTITLE
Electron and Proton Wide-Angle Spectrometer (EPAS) on the CRRES Spacecraft

5. FUNDING NUMBERS
F04701-88-C-0089

6. AUTHOR(S)
Korth, A., Kremser, G., Wilken, B., and Güttler, W. (Max-Planck-Institut);
Ullaland, S. L. (University of Bergen); and Koga, R. (The Aerospace Corporation)

7. PERFORMING ORGANIZATION NAME(S) AND ADDRESS(ES)
The Aerospace Corporation
Technology Operations
El Segundo, CA 90245-4691

8. PERFORMING ORGANIZATION REPORT NUMBER
TR-0091(6940-05)-11

9. SPONSORING/MONITORING AGENCY NAME(S) AND ADDRESS(ES)
Space and Missile Systems Center
Air Force Materiel Command
2430 E. El Segundo Blvd.
Los Angeles Air Force Base, CA 90245

10. SPONSORING/MONITORING AGENCY REPORT NUMBER
SMC-TR-94-15

11. SUPPLEMENTARY NOTES

12a. DISTRIBUTION/AVAILABILITY STATEMENT
Approved for public release; distribution unlimited

12b. DISTRIBUTION CODE

13. ABSTRACT (*Maximum 200 words*)

The electron and proton wide-angle spectrometer (EPAS) in the CRRES scientific payload utilizes arrays of solid-state detectors coupled with a magnetic deflection system in order to detect electrons (21-285 keV) and protons (37-3200 keV). The image size of the particles and the angular resolutions are controlled by the width of the entrance hole, the geometry of the pole pieces, and the position of the particles in the image plane. Additional features of the EPAS are described in some detail. Selected in-flight data are shown as an illustration of the instrument performance in the operational orbit.

14. SUBJECT TERMS
CRRES (Combined Release and Radiation Effects Satellite)
Electrons in Magnetosphere, Magnetosphere, Protons in Magnetosphere, Space Instrumentation

15. NUMBER OF PAGES
10

16. PRICE CODE

17. SECURITY CLASSIFICATION OF REPORT	18. SECURITY CLASSIFICATION OF THIS PAGE	19. SECURITY CLASSIFICATION OF ABSTRACT	20. LIMITATION OF ABSTRACT
Unclassified	Unclassified	Unclassified	

CONTENTS

I. Scientific Objectives 2

II. Instrument Design 2

III. Analog Electronics 3

IV. Instrument Calibration with an Electron Beam 4

V. Performance After Launch 4

Acknowledgments 5

References 5

FIGURES

1. Schematic drawing of one unit of the spectrometer with a 60-deg opening collimator and an array of five electron detectors and two ion telescopes 2

2. Look directions of the electron and proton (ion) detectors with respect to the spacecraft spin axis 3

3. Block diagram of the analog electronics 4

4. Differential electron intensities in 12 energy channels from detector E7 and ion intensities in ten energy channels from detector P2 during CRRES orbit 106 5

5. Integral electron intensities and proton intensities in a time vs pitch-angle diagram from CRRES orbit 73 5

I. Scientific Objectives

ENERGETIC particles are sensitive probes of the global state of the magnetosphere. Complete energy spectra and pitch-angle distributions of energetic particles can be used to identify the mechanisms of access, acceleration, transport, and loss of energetic charged particles in the magnetosphere. Certain unique features of the combined release and radiation effects satellite (CRRES) orbit favor the investigation of these mechanisms on the dayside as well as in the near-Earth tail.

The CRRES orbit provides encounters with the dayside magnetopause during large magnetospheric disturbances and thus enables the study of magnetospheric boundary phenomena. Transport of particles across the magnetopause may arise through wave-particle interactions,[1] steady reconnection,[2] sporadic reconnection,[3] or flux transfer events.[4] Using analytic methods,[5] we intend to monitor themagnetopause position, its orientation, and motion whenever the satellite is in the magnetosphere within a few hundred kilometers of the magnetopause.

The $6.2R_E$ apogee can also provide detailed observations of the substorm development near the equatorial plane. Current substorm models can be examined. Many observations are in agreement with models in which the substorm is triggered in the near-Earth region ($10–20R_E$) of the plasma sheet by the formation of a neutral line at which magnetic field reconnection suddenly takes place.[6] But there are also observations which show that the substorm may be triggered as close to the Earth as the geosynchronous orbit.[7,8] Roux et al.[8] interpreted these observations in terms of a surface wave generated by a plasma instability in the transition region between more dipolar and more tail-like geomagnetic field lines.

Another aspect is the influence of storm sudden commencements on the particle distribution[9,10] as well as their role in the substorm triggering.[11]

Interactions of particles with waves are important for the coupling of the magnetosphere with the ionosphere. The waves are needed to scatter field-aligned ionospheric particles onto trapped orbits. Conversely, waves act to precipitate particles into the ionosphere. We will examine the effect of different plasma waves on particle precipitation. We will also study the effects of ion-cyclotron waves on protons.

The instrument focuses, furthermore, on studies of the natural radiation environment, their dynamics, and their dependence on the solar activity.

To investigate these processes, high-resolution three-dimensional particle distributions have to be measured. The electron and proton wide-angle spectrometer (EPAS) is well suited for this purpose. It covers the energy range for electrons from 21–285 keV and for protons from 37 ke V–3.2 MeV.

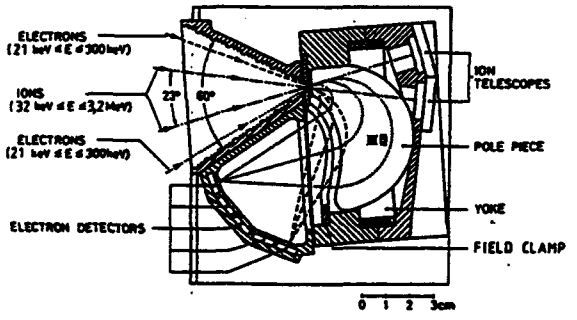

Fig. 1 Schematic drawing of one unit of the spectrometer with a 60-deg opening collimator and an array of five electron detectors and two ion telescopes.

Table 1 EPAS instrument parameters

	Electrons (E0–E9)	Protons (P0–P3)
Energy range	21–300 keV	32–3200 keV
Integral energy channels	>25.5 keV	>32.0 keV
Differential energy channels	1. 21.0–31.5 keV 2. 31.5–40.0 keV 3. 40.0–49.5 keV 4. 49.5–59.0 keV 5. 59.0–69.0 keV 6. 69.0–81.0 keV 7. 81.0–94.5 keV 8. 94.5–112.0 keV 9. 112.0–129.5 keV 10. 129.5–151.0 keV 11. 151.0–177.5 keV 12. 177.5–208.0 keV 13. 208.0–242.5 keV 14. 242.5–285.0 keV	1. 37–54 keV 2. 54–69 keV 3. 69–85 keV 4. 85–113 keV 5. 113–147 keV 6. 147–193 keV 7. 193–254 keV 8. 254–335 keV 9. 335–447 keV 10. 447–602 keV 11. 602–805 keV 12. 805–3200 keV
Look directions of detectors with respect to the spin axis	20 deg (E0); 30 deg (E1) 40 deg (E2); 50 deg (E3) 60 deg (E4); 70 deg (E5) 80 deg (E6); 90 deg (E7) 100 deg (E8); 110 deg (E9)	26 deg (P0) 46 deg (P1) 87 deg (P2) 107 deg (P3)
Angular resolutions in elevation in azimuth	±3 deg ±2 deg	±5 deg ±2 deg
Geometric factor	$\approx 5\times10^{-5}$ cm²sr	2.0×10^{-4} cm²sr
Total weight	4.06 kg	
Total power	2.65 W (average)	

II. Instrument Design

EPAS consists of two identical units to measure electrons simultaneously in ten directions and ions in four directions over a total angular range of ≈110 deg. Each unit contains a magnetic deflection system and an array of solid-state detectors (Fig.1). Particles entering the spectrometer encounter a homogeneous magnetic field of 0.08 T which separates protons and heavier ions from electrons. The magnetic field geometry was designed such that a parallel beam of electrons entering the instrument at a given angle with respect to the axis of the aperture is deflected and focused to a single point irrespective of its energy. The deflection system thus defines a focal curve on which each point corresponds to a given angle of incidence to the spectrometer. Along this focal curve, five rectangular solid-state detectors are mounted which define five angular intervals within the 60–deg aperture of the unit. The focusing can be achieved for electrons with energies between 15 and 300 keV.

The finite width of the entrance hole, the geometry of the pole pieces, and the position of the detectors in the image plane define both the image size of monoenergetic electrons and the angular resolution for the velocity focusing. The angle α (in the elevation direction with respect to the spin axis) is given by the size of the detectors, whereas the angle β (azimuthal direction around the spin axis) is limited by the mechanical aperture to a few degrees (see Table 1) to effectively suppress electron scattering from the pole pieces.

The influence of the fringing magnetic field at the entrance hole and where the electrons exit the sector field can have an important effect on the image aberration. To minimize this effect, a magnetic field clamp is introduced which suppresses the fringing field. The entrance hole has a diameter of 1.2 mm which is approximately the upper limit required by the electron optical properties of the magnet. The transmission of the incident electrons through the magnetic system is a function of the particle energy and the angles of incidence α and β. To

evaluate the focusing properties extensive calibrations were performed (see Sec. IV).

The electrons are detected with rectangular, totally depleted silicon surface barrier detectors. The active area is $5 \times 10\ mm^2$, and the thickness is 300 μm which is sufficient to absorb electrons with energies up to 300 keV. The Al-side of the detectors is facing the incoming particles. This side is made light tight by using a layer of 120 $\mu g/cm^2$ of Al. The total energy range is divided into 14 approximately logarithmically spaced energy channels that are called differential energy channels (see Table 1).

The deflection of ions with energies above 20 keV is negligible. They move on almost straight lines and are detected in solid-state detector telescopes (Fig. 1). For each unit, two telescopes are mounted behind the magnetic deflection system and define two directions for the measurement of ions. Each telescope consists of a front and a back solid-state detector. The front detector has a sensitive area of 50 mm^2 and is used for the energy analysis of ions; the back detector (sensitive area of 100 mm^2) provides a veto signal to reject penetrating particles. The front detector of the telescope is operated with the aluminium contact facing the environment. This has two reasons: 1) the Al-contact can be made as thin as 15 $\mu g/cm^2$, and 2) the detector lifetime against radiation damage is increased by two or more orders of magnitude in total ion exposure. The energy loss in the dead layer depends on the ion species and its energy. It amounts to about 7–8 keV for protons with an energy of 20 keV. The energy loss is determined at various energies from measurements in the Max-Planck-Institut für Aeronomie (MPAe) ion-accelerator and is included in the energy channels for protons (see Table 1).

The upper energy range of the telescope is defined by the thickness of the front detector, which amounts to 100 μm, and thus covers the energy range up to about 3.2 MeV for protons. The total energy range is divided into 12 approximately logarithmically spaced energy channels.

No identification of the ion species is possible. Since the energy losses in the dead layer increase with Z, we expect a contribution of less than 10% to the count rate of the instrument by ions with $Z \geq 2$ during quiet to moderately disturbed periods. This estimate is based on a comparison of measurements by the electron-proton spectrometer and the ion mass spectrometer on the spacecraft GEOS-1 and -2.

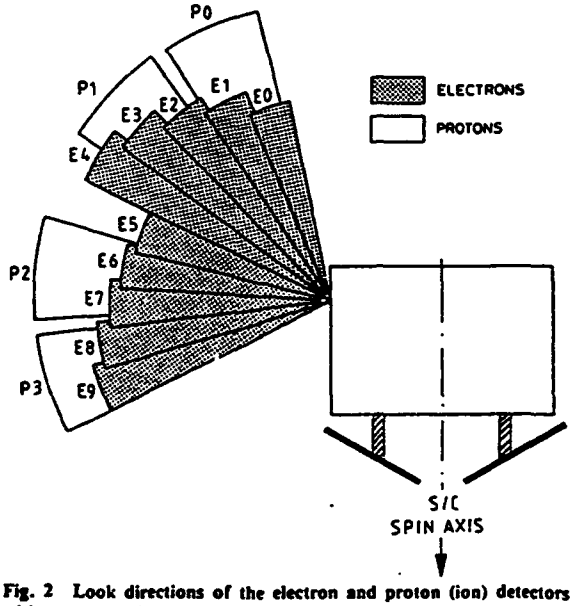

Fig. 2 Look directions of the electron and proton (ion) detectors with respect to the spacecraft spin axis.

Because of the deflection in the magnetic field, electrons with energies below 800 keV cannot reach the proton telescopes. Electrons with higher energies penetrate the front detector, provide a veto signal in the back detector, and are rejected. For this reason, the lowest energy threshold for the protons is essentially given by the noise of the front detector and the analog electronics.

The spectrometer uses $SmCo_5$ as magnetic material. The yoke and the pole pieces are made from magnetically soft iron with a very small coercitive force and high permeability. In order not to disturb magnetic field sensors or other instruments sensitive to magnetic fields on the spacecraft, the magnetic system is completely enclosed by a shielding can of high-permeability material (μ-metal). The shielding factor (ratio of the internal and external field) of such a system is a complicated function of the magnetic permeability, the shape, the size, and the wall thickness. It can only be derived from measurements. A satisfactory attenuation was achieved after a careful annealing process of the soft iron material and after the positioning of the two units in such a way that the magnetic fields between the pole pieces have opposite directions. In this position, the dipole fields cancel each other and only stray fields of higher order will remain. The measured maximum value of the residual field was 2 nT at a distance of 50 cm from the center of the sensor system.

The sensor is thermally isolated from the analog electronics, since the detectors have to be operated at a lower temperature than the electronics. In fact, the detector noise can be substantially reduced if the detectors are operated at temperatures between $-20°C$ and $+5°C$. Therefore the front of the sensor which is facing the outside environment is designed as a radiator. Small electrically conducting second surface mirrors are fixed to the sensor to radiate the heat into space. From measurements during the solar simulation tests we expect sufficiently low sensor temperatures.

The EPAS spectrometer contains two of the described units and covers in total an angular range of ≈ 110 deg. The sensor is mounted on the platform of the spacecraft and is directed such that the angular range of 110 deg is located in the meridian plane of the satellite. The spectrometer is able to detect electrons simultaneously from ten directions and protons from four directions (Fig. 2). The spin axis of the CRRES spacecraft is located in the orbital plane.

The three-dimensional directional distribution can be converted into a pitch-angle distribution with the help of the magnetic field measurements on the same satellite. The pitch angle is a function of the local magnetic field vector with respect to the spin axis and the look directions of the different detectors.

III. Analog Electronics

The analog electronics box is mechanically connected to the sensor box, but electrically and thermally isolated from it. The analog box consists of many individual housings to achieve a careful shielding between the amplifier chains and thus to avoid cross talk. The electrical interface between the analog box and the data processing unit (DPU) only allows the transmission of digital pulses.

The functional block diagram of the analog electronics of the EPAS instrument is shown in Fig. 3. All solid state detectors (protons: P0–P3; electrons: E0–E9) are followed by charge-sensitive preamplifiers, pulse amplifiers, pulse formers, and discriminators.

The ion telescopes produce three different sets of data: the count rates of the front detectors (P0–P3), the count rates of the back detectors (U0–U3), and coincidence counts of the front and back detectors. The count rates of the front detectors go to a "Proton Selector" unit that selects one out of the four detectors for energy analysis in the proton pulse-height analyzer (PHA). This analysis is only carried out if a coincidence between front and back detectors has not occurred. These data are called differential count rates. The energy thresholds are given in Table 1. Simultaneously the count rates

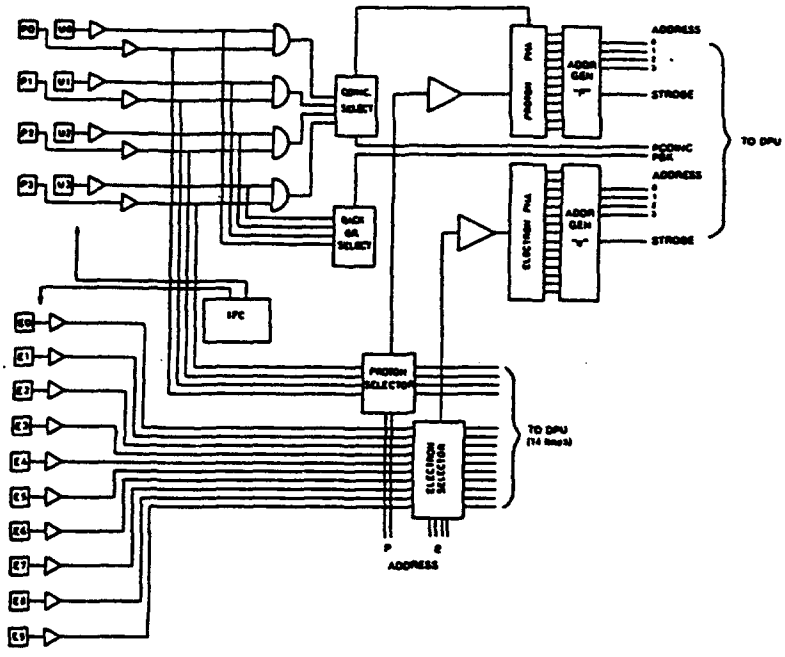

Fig. 3 Block diagram of the analog electronics.

of the four front detectors are routed via discriminators to the DPU; these are called integral count rates. The energy thresholds are given in Table 1.

The data lines from the ten electron detectors (E0–E9) pass the "Electron Selector" that determines on which of the ten channels energy analysis is carried out in the electron PHA. The ten data lines are also routed via discriminators as integral count rates directly to the DPU.

The proton and electron PHAs sort the count rates from one selected proton and from one electron detector into 12 or 14 different energy intervals, respectively. The differential count rates are taken consecutively from the various electron and proton detectors. The sampling time for the protons amounts to 512 ms and for the electrons to 256 ms. During the normal mode, the proton detector sequence is P2, P0, P1, P3, P2, P0; P2, . . .; and the electron detector sequence is E6, E9, E2, E7, E4, E0, E6, E8, E1, E5, E3, E0; E6, . . . These sequences can be changed by command.

The integral count rates are obtained simultaneously for all detectors. The time resolution for the integral count rates of electrons and protons amounts to 512 ms.

An in-flight test generator (IFC) is used to control the operation of the instrument. Pulses with varying amplitudes are fed into the inputs of the charge-sensitive amplifiers and are counted at the outputs of the two PHAs as well as at the outputs of the discriminators. The in-flight calibrator is initiated via the IFC ON line and controlled by the frequency of the IFC clock.

The DPU provides 16 scalers to monitor the integral counting rates from the ten electron detectors, four proton front detectors, and coincidence and back detector counting rates of the proton detector selected for pulse-height analysis. Two scalers in the DPU are driven by two sets of 4-bit address and single strobe lines, one each for the proton and electron detector selected for pulse-height analysis. The DPU contains power supplies to provide power to the sensor with various voltages. Details of the DPU are published in this volume.[12]

IV. Instrument Calibration with an Electron Beam

In general, the transmission of incident electrons through the magnetic system shown in Fig. 1 is a function of particle energy and the incidence angles α and β. The detection efficiency depends on the active area and relevant parameters of the detector.

To evaluate the focusing properties quantitatively and therewith the transmission efficiency, the complete system was calibrated with electrons in the energy range of $20 \leq E \leq 150$ keV supplied by an electrostatic accelerator and in the energy range of $70 \leq E \leq 400$ keV using electrons from a Van-de-Graaf generator. (Both the accelerator and the generator are facilities of the Goddard Space Center, Greenbelt, Maryland.) The experiment was mounted on a platform allowing rotations around two axes perpendicular to each other to define the angles of incidence α and β. The accuracy for both angles was 0.1 deg. The alignment of the experiment in the vacuum chamber with respect to the center of the beam line was achieved by optical autocollimation. The beam diameter was 15 mm, which is much larger than the aperture diameter of 1.2 mm. A monitor detector was mounted on a mechanical device and could be moved directly in front of the collimator. The aperture diameter of the monitor detector was 2.0 mm. The response of the monitor detector was used to inspect the spectral shape of the beam and to normalize the response of the magnetic system.

The signals generated in the five electron detectors were processed with individual amplifier-discriminator-counter chains allowing simultaneous measurements from all detectors. A PHA was used to take spectra routinely from each detector in order to detect spectral distortions due to scattering in the instrument.

The counting rates from detectors E0–E9 and the monitor detector were used to determine the transmission efficiency. The spectral information was used to correct scattering effects and system noise.

For the flight data analysis, we will use from the calibration measurements two two-dimensional tables which give 1) actual look directions for all electron detectors vs energy channels and 2) geometric factors for all electron detectors vs energy channels. Average values are given in Table 1.

V. Performance After Launch

The EPAS instrument on CRRES has been operating successfully since launch. The instrument design temperatures were achieved. The operating temperatures reached $-20°C$

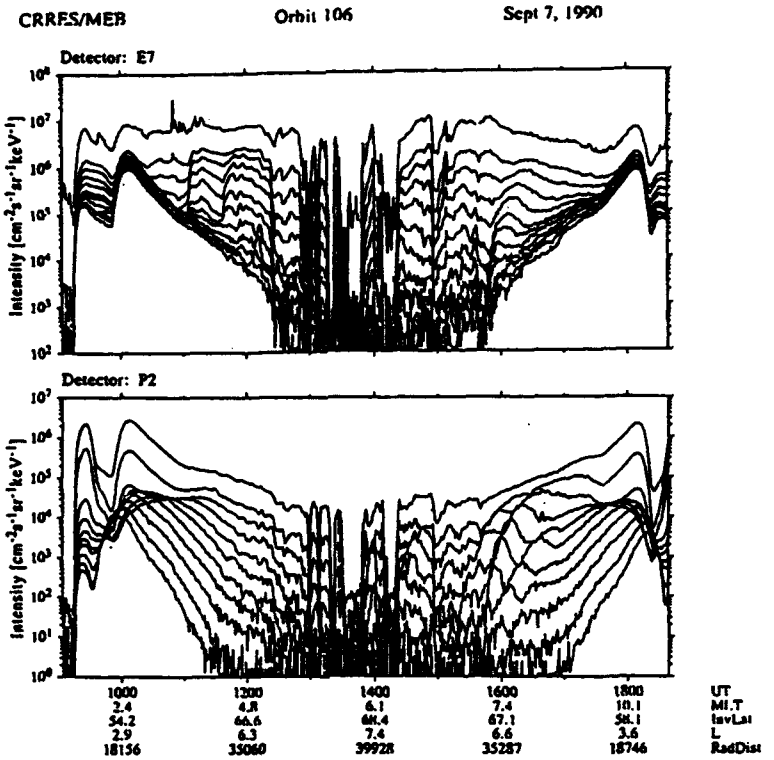

Fig. 4 Differential electron intensities in 12 energy channels from detector E7 and ion intensities in ten energy channels from detector P2 during CRRES orbit 106.

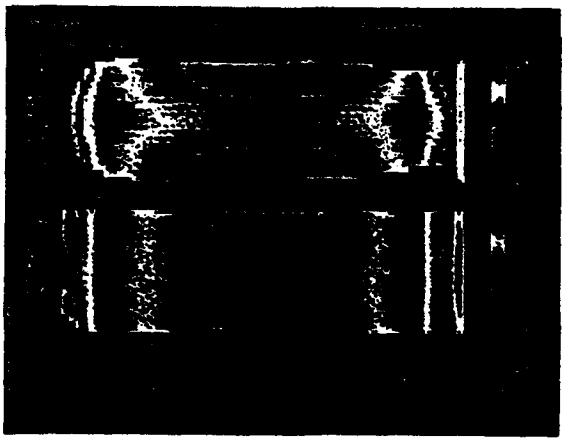

Fig. 5 Integral electron intensities ($E > 25.5$ keV) and proton intensities ($E > 32$ keV) in a time vs pitch-angle diagram from CRRES orbit 73.

for the sensor and +6°C for the analog electronics. The detector noise levels were comparable to the values measured on ground.

Fig. 4 displays the intensities measured in 12 differential energy channels of the electron detector E7 and ten differential energy channels of the proton detector P2 during the CRRES orbit 106. The data were averaged over 1 min. The lowest energy channel is displayed on top of each panel and is given as first channel in Table 1. Near $L = 6$ several dropout events were observed. During these events the count rates dropped to zero and the detector noise level could be determined, especially for the lowest differential electron and proton channels.

A second example of the instrument performance is shown in Fig. 5. The integral electron ($E > 25.5$ keV) and ion ($E > 32$ keV) intensities are displayed in a time vs pitch-angle diagram. The data were obtained during orbit 73 and were averaged over 1 min. The intensity is given in a color coded logarithmic scale. During this orbit the magnetosphere was not disturbed. The inner and outer radiation belts together with the slot region are clearly identified.

Acknowledgments

The MEB spectrometer was designed and constructed with support from the Max-Planck Gesellschaft zur Förderung der Wissenschaften. Grants were received from the United States Air Force under AFOSR-85-0237 and from the Norwegian Research Council for Science and the Humanities to the University of Bergen. The data processing unit and instrument integration were supported at The Aerospace Corporation under Air Force Space Systems Division Contract F04701-88-C-0089.

References

[1]Eviatar, A., and Wolf, R. A., "Transfer Processes at the Magnetopause," *Journal of Geophysical Research*, Vol. 73, No. 17, 1968, p. 5561-5576.

[2]Korth, A., Kremser, G., and Daly, P. W., "Observations of Field-Aligned Energetic Electron and Ion Distributions Near the Magnetopause at Geosynchronous Orbit," *Journal of Geophysical Research*, Vol. 87, No. A12, 1982, pp. 10,413-10,419.

[3]Paschmann, G., et al., "Plasma Acceleration at the Earth's Magnetopause: Evidence for Reconnection," *Nature*, Vol. 282, Nov. 1979, pp. 243-246.

[4]Russell, C. T., and Elphic, R. C., "Initial ISEE Magnetometer Results: Magnetopause Observations," *Space Science Reviews*, Vol. 22, No. 6, 1978, pp. 681-715.

[5]Williams, D. J., Fritz, T. A., Wilken, B., and Keppler, E., "An Energetic Particle Perspective of the Magnetopause," *Journal of Geophysical Research*, Vol. 84, No. A11, 1979, pp. 6385-6396.

[6]Baker, D. N., Akasofu, S.-I., Baumjohann, W., Bieber, J. W., Fairfield, D. H., Hones, E. W., Jr., Mauk, B., McPherron, R. L., and Moore, T. E., "Substorms in the Magnetosphere, Solar Terrestrial Physics: Present and Future," *NASA Ref. Publ.*, pp. 1120–1128, Chap. 8, 1984.

[7]Kremser, G., Korth, A., Ullaland, S. L., Perraut, S., Roux, A., Pedersen, A., Schmidt, R., and Tanskanen, P., "Field-Aligned Beams of Energetic Electrons (16 keV $\leq E \leq$ 80 keV) Observed at Geosynchronous Orbit at Substorm Onsets," *Journal of Geophysical Research*, Vol. 93, No. A12, 1988, pp. 14,453–14,464.

[8]Roux, A., Perraut, S., Robert, P., Morane, A., Pedersen, A., Korth, A., Kremser, G., Aparicio, B., Rodgers, D., and Pellinen, R., "Plasmasheet Instability Related to the Westward Travelling Surge," *Journal of Geophysical Research*, Vol. 96, No. A10, 1991, pp. 17,697–17,714.

[9]Korth, A., Kremser, G., Cornilleau-Wehrlin, N., and Solomon, J., "Observations of Energetic Electrons and VLF Waves at Geostationary Orbit During Storm Sudden Commencements (SSC)," *Solar Wind-Magnetosphere Coupling*, edited by Y. Kamide and J. A. Slavin, Terra Scientific Publishing Co., Tokyo, Japan, 1986, pp. 391–399.

[10]Wilken, B., Baker, D. N., Higbie, P. R., Fritz, T. A., Olsen, W. P., and Pfitzer, K. A., "Magnetospheric Configuration and Energetic Particle Effects Associated with a SSC: A Case Study of the CDAW 6 Event on March 22, 1979," *Journal of Geophysical Research*, Vol. 91, No. A2, 1986, pp. 1459–1473.

[11]Ullaland, S. L., Kremser, G., Tanskanen, P., Korth, A., Torkar, K., Block, L., and Iversen, I. B., "Influence of a Storm Sudden Commencement on the Development of a Magnetospheric Substorm: Ground, Balloon, and Satellite Observations," *Journal of Geophysical Research*, (submitted for publication), 1992.

[12]Koga, R., Imamoto, S. S., Katz, N., Pinkerton, S. D., "Data Processing Units for Eight Magnetospheric Particle and Field Sensors," *Journal of Spacecraft and Rockets*, Vol. 29, No. 4, 1992, pp. 574–579.

TECHNOLOGY OPERATIONS

The Aerospace Corporation functions as an "architect-engineer" for national security programs, specializing in advanced military space systems. The Corporation's Technology Operations supports the effective and timely development and operation of national security systems through scientific research and the application of advanced technology. Vital to the success of the Corporation is the technical staff's wide-ranging expertise and its ability to stay abreast of new technological developments and program support issues associated with rapidly evolving space systems. Contributing capabilities are provided by these individual Technology Centers:

Electronics Technology Center: Microelectronics, solid-state device physics, VLSI reliability, compound semiconductors, radiation hardening, data storage technologies, infrared detector devices and testing; electro-optics, quantum electronics, solid-state lasers, optical propagation and communications; cw and pulsed chemical laser development, optical resonators, beam control, atmospheric propagation, and laser effects and countermeasures; atomic frequency standards, applied laser spectroscopy, laser chemistry, laser optoelectronics, phase conjugation and coherent imaging, solar cell physics, battery electrochemistry, battery testing and evaluation.

Mechanics and Materials Technology Center: Evaluation and characterization of new materials: metals, alloys, ceramics, polymers and their composites, and new forms of carbon; development and analysis of thin films and deposition techniques; nondestructive evaluation, component failure analysis and reliability; fracture mechanics and stress corrosion; development and evaluation of hardened components; analysis and evaluation of materials at cryogenic and elevated temperatures; launch vehicle and reentry fluid mechanics, heat transfer and flight dynamics; chemical and electric propulsion; spacecraft structural mechanics, spacecraft survivability and vulnerability assessment; contamination, thermal and structural control; high temperature thermomechanics, gas kinetics and radiation; lubrication and surface phenomena.

Space and Environment Technology Center: Magnetospheric, auroral and cosmic ray physics, wave-particle interactions, magnetospheric plasma waves; atmospheric and ionospheric physics, density and composition of the upper atmosphere, remote sensing using atmospheric radiation; solar physics, infrared astronomy, infrared signature analysis; effects of solar activity, magnetic storms and nuclear explosions on the earth's atmosphere, ionosphere and magnetosphere; effects of electromagnetic and particulate radiations on space systems; space instrumentation; propellant chemistry, chemical dynamics, environmental chemistry, trace detection; atmospheric chemical reactions, atmospheric optics, light scattering, state-specific chemical reactions and radiative signatures of missile plumes, and sensor out-of-field-of-view rejection.